Coupling flow, heat and reactive transport modelling to reproduce *in-situ* redox potential evolution: application to an infiltration pond

Paula Rodríguez-Escales[1,2*], Carme Barba[1,2], Xavier Sanchez-Vila [1,2], Diederik Jacques[3], Albert Folch [1,2,4]

1 Dept. of Civil and Environmental Engineering. Universitat Politècnica de Catalunya, Jordi Girona 1-3, 08034 Barcelona, Spain;

2 Associated Unit: Hydrogeology Group (UPC-CSIC);

3 Engineered and Geosystems Analysis, Institute for Environment, Health and Safety, Belgian Nuclear Research Centre, Boeretang 200, Mol, 2400, Belgium

4 Serra Hunter Fellow

*Corresponding author: paula.rodriguez.escales@upc.edu

Abstract

Redox potential (Eh) measurements are widely used as indicators of the dominant reduction-oxidation reactions occurring underground. Yet, Eh data are mostly used in qualitative terms, as actual values cannot be used to distinguish uniquely the dominant redox processes at a sampling point, and should therefore be combined with a detailed geochemical characterization of water samples. In this work, we have intensively characterized the redox potential of the first meter of soil in an infiltration pond recharged with river water using a set of *in-situ* sensors measuring every 12 min during a one-year period. This large amount of data combined with hydrogeochemical campaigns allowed developing a reactive transport model capable of reproducing the redox potential in space and time together with the site hydrochemistry. Our results showed redox processes were mainly driven by the amount of Sedimentary Organic Matter in the system as well as by seasonal variation of temperature. As a subsidiary result, our work emphasizes the need to use a fully coupled model of flow, heat transport, solute transport and the geochemical reaction network to fully reproduce the Eh observations in the topsoil.

TOC Art

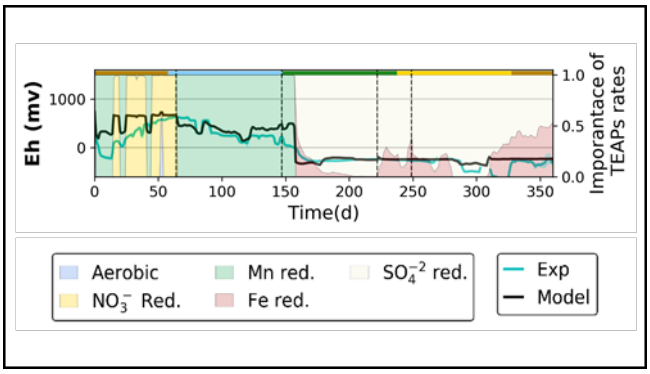
Eh (mv)
1000
0
0
50
100
150
200
250
300
350
Time(d)
1.0
0.5
0.0
Imporantace of TEAPs rates
Aerobic
Mn red.
SO_4^{-2} red.
NO_3^- Red.
Fe red.
Exp
Model

1 Introduction

The determination of the reduction-oxidation (redox) potential (Eh) in water bodies is a common practice to characterize the biogeochemistry of water samples. The redox state determines the distribution of all redox equilibria; thus, similarly to pH, it can be considered as a quantity that lumps multiple processes occurring simultaneously at the corresponding sampling point in the subsurface[1]. Currently, the individual Eh measurements do not provide univocal information to characterize the dominant redox processes at a particular location. Therefore, it is only considered as a line of evidence in the dominant processes identification that would, otherwise, mostly rely on measuring the concentrations of redox-sensitive groundwater constituents[2, 3]. There are different reasons why the redox potential cannot be used as a quantitative parameter. Firstly, the mixed potentials due to the lack of equilibrium between the different redox couples in any water sample[2], which hinders the determination of redox couple concentrations from the Nernst equation. Secondly, field Eh is typically measured with a sensor probe embedded in a flow cell from pumped water. In subsurface systems with steep redox gradients (e.g., hyporheic zones or infiltration areas), or highly heterogeneous, these measured Eh values are not representative, as point samples integrate a mixture of waters present at the capture zone of the monitoring point. Regarding the Eh measurments reproducibility, a reactive transport model would require the consideration of all primary and secondary processes controlling the redox state: reduction of all aqueous or mineral-form Terminal Electron Acceptors (TEAPs), oxidation of electron donors (such as organic matter), solute and heat transport, and secondary geochemical processes (not necessarily involving any electron transfer) still impact reaction pathways and rates of the primary redox reactions.

Sensors capable of measuring the redox potential at a single point[4] are an alternative to flow cell sampling. Its use, which is increasing, avoids the mixing interferences and can catch the redox evolution in highly dynamic systems (e.g. wetlands[5], aquifer-stream interaction[6], or constructed delta-lake systems[7]). Sensor data could be directly integrated into the model-based analysis of biogeochemical subsurface systems, adding significant value to field Eh data. Note that measuring Eh is not expensive, as it can be determined by potentiometric measurements with a non-intrusive and continuous sensor, whereas hydrogeochemical analyses are intrusive, non-continuous and time consuming.

Surface infiltration ponds are highly dynamic redox systems[8-10]. They are a type of managed aquifer recharge (MAR) facilities, aimed at increasing the availability of groundwater resources by storing water in the subsurface and increasing the residence time to enhance opportunities for kinetically controlled water purification processes[11, 12]. Redox reactions are driven by the simultaneous availability of TEAPs-containing waters and electron donors, thus contributing to the degradation of nutrients (dissolved organic carbon[13, 14], nitrates[8, 15-17]) and organic pollutants[18-22]. Consequently, redox processes are dominant in these systems and a key aspect in the purification capacity of infiltration ponds[20, 23].

Most typically, the limiting component of a redox reaction is the concentration of the electron donor (typically, organic carbon)[24]. In MAR facilities, organic matter can be supplied by the recharge water, but it can also be generated in the recharge system itself from the fixation of CO_2 by the photosynthetic organisms (algae, cyanobacteria and plants)[25]. The growth of these organisms depends on temperature, light conditions, and availability of inorganic nutrients (N,P)[26] and it is specially high during warm periods, resulting in algae blooms and surface bioclogging[27,28]. Consequently, temperature is also a key aspect controlling redox reactions[9, 29].

The spatio-temporal evolution of the *Eh* is an integrated value of all the geochemical processes involved. In this way, a geochemical model capable of reproducing the *Eh* data should also be integrative. Although some works have focused on modelling redox processes in MAR[9, 30-34], to our knowledge there is none integrating all the mentioned processes to understand and reproduce the spatial and temporal evolution of *Eh* data, mostly in the topsoil first meter, where most of the redox and biological processes occur[10, 35]. Note that understanding the redox temporal and spatial dynamic in an infiltration pond model will allow to understand, improve and optimize the purification capacity of an infiltration facility, especially regarding the recalcitrant compounds like Emerging Organic Contaminants that are degraded by co-metabolism depending on the redox reactions[20-22].

Thus, this work is aimed at developing a reactive transport model to reproduce the *Eh* values measured in a real system. The model will integrate all the processes affecting the redox potential in a managed aquifer recharge facility in order to establish a method to reproduce the *Eh* in a numerical model. The model development was constrained by one-year data from continuous *in-situ* redox potential sensors collected in an infiltration pond facility.

2 Methodology

2.1 Field site and monitoring network description

The Castellbisbal recharge facility is located in the conurbation of Barcelona (Spain). It is composed by a permanent-regime wetland (14,500 m^2) and an infiltration pond (1,400 m^2). The recharge water comes from the Llobregat River. Site description,

109 construction and hydrogeological details are provided in Section 1 in the Supporting
110 Information (SI).

111 The site was intensively monitored during one year (from 25/10/2016 to 24/10/2017)
112 by continuous and non-intrusive sensors (pressure, temperature and redox potential)
113 located within the infiltration pond at different points and depths (Figure S1),
114 complemented by four sampling campaigns performed during the monitoring year
115 for geochemical analyses. Eh measurements were recorded every 12 min (a dataset
116 of 43,800 values per sampling point) using platinum redox sensors 1 mm thick
117 located along stick probes (Hypnos III, MVH Consult). Measurements were taken in
118 10 points located at the pond surface and at different depths: ~20 cm, ~50 cm, ~60
119 cm, and ~70 cm (See Figure S1c). An extra sensor was placed inside piezometer PJ,
120 where the reference electrode (Ag/AgCl) was also installed at 6 m depth to ensure
121 permanent wet conditions. Both depth and plain view distribution of the sensor
122 probes and sampling points are displayed in Figure S1c. Two temperature sensors
123 were integrated into the redox probes, one at the water pond (probe 1) and the other
124 one at a depth of 55 cm (probe 3, Figure S1c). See SI for more detailed information.

125 The four sampling campaigns were distributed along the monitored year in order to
126 cover the seasonality as well as operational tasks affecting the infiltration rates,
127 especially scrapping operations. The first campaign took place in winter (December
128 2016); the second in spring (April 2017); the third, right after a scrapping operation
129 following a significant (bio)clogging event detected in June 2017; the last one, in
130 summer (July 2017). The pond remained empty during summer holidays (August
131 2017). Water samples were taken at different locations: 1) infiltration pond, 2)
132 different depths within the vadose zone (20, 50 and 90 cm), and 3) the aquifer just
133 below the infiltration pond (PJ) (see Figure S1.c). At each sampling point, some field
134 parameters (Temperature, pH, Eh, dissolved oxygen, alkalinity), and the

concentration of the main hydrogeochemical compounds (dissolved organic carbon, major cations, anions, nutrients and metals) were obtained. The specific mineralogy of the sediments and the total iron and manganese from two random points at 30 cm depth within the infiltration pond were determined. During the sampling campaigns, we also determined the total amount of organic matter in five random points within the first 2 cm of the sediment at the infiltration pond. All the detailed information of sampling and chemical determination is available in SI (Section S2).

2.2 Reactive transport modeling: processes and governing equations

A one-dimensional flow, heat and reactive transport model of the infiltration pond for the Castellbisbal site was constructed using HP1[36, 37] (Hydrus[38] + PHREEQC[39]). The model solves the Richards' equation for flow and the convection-dispersion-reaction equation for heat and reactive transport (see section S3 of SI for equation details and model assumptions).

Figure 1 shows all the hypothesized and key reactive processes affecting Eh in the infiltration pond, and consequently, included in the geochemical model (see also Table 1). The processes included were chosen accordingly to the observation data and literature review. Process 1 relates to the organic matter generation (from the decomposition of algae and cyanobacteria) and its degradation to dissolved organic carbon (DOC) and ammonium (process 2). Then, DOC oxidizes using different TEAPs to inorganic carbon (process 3), which is equilibrated to different forms of carbon depending on the pH of the system and the carbonate/CO_2 equilibria. The ammonium released during organic matter mineralization and ammonium contained in the recharged water are concurrently oxidized to nitrate; however, solely under aerobic conditions (nitrification, process 4). Nitrate is reduced to dinitrogen gas, coupled to organic carbon oxidation (dashed line, process 3). The

160 intermediate production of nitrite during both nitrification and denitrification was
161 not considered as no nitrite was measured in any sample. Note that sulfate reduction
162 can also occur due to the re-oxidation of Fe^{+2}[40]. Goethite was selected as
163 representative of the Fe^{+3} phase. Mineral reactions involving calcite, rhodochrosite
164 ($MnCO_3$), siderite ($FeCO_3$), and mackinawite (FeS) (processes 5 to 8, respectively), as
165 well as cation exchange of manganese and iron with soil phases (e.g., clay and
166 organic matter; process 9), were also included in the model.

167 All the mentioned processes were considered as kinetically controlled (Table 1),
168 which avoided mixed potential and irreversibility in redox processes[41], with the
169 exception of siderite formation (6), the exchange processes (9) and speciation
170 reactions (such inorganic carbon equilibrium) for which the local equilibrium
171 assumption (LEA) was implemented.

172 Seven cations (Na^+,K^+, NH_4^+, Ca^{+2}, Mg^{+2}, Mn^{+2}, Fe^{+2}) were competing for one
173 exchanger site. Equilibrium constants for cation exchange and for aqueous
174 speciation reactions were taken from the PHREEQC database.

175 All processes related to DOC were temperature dependent following the expression
176 of O'Connell et al. (1990)[42] (see F_T, Table 1), already implemented in MAR studies[9].
177 Regarding the temperature effect in mineral formation, we assumed an Arrhenius
178 dependence ($F_{T_{Ar}}$)[1, 43]. All the equation details and the parameter description are
179 available in SI (Section S3).

180 Conceptually, Eh indicates the tendency of an environment to exchange (receive or
181 give) electrons. Aqueous systems contain no free electrons, but the relative electron
182 activity, as an intensity parameter, can still be defined, as $pe = -\log[e^-]$. Thus, Eh
183 is related to pe and to the concentration of the redox pairs, by means of the equation
184 $h = \frac{2.3RTpe}{F}$, where R is the gas constant, T is temperature and F the Faraday's

185 constant. In order to evaluate electron activity in quantitative terms, PHREEQC
186 assumes, as a starting point, a redox equilibrium which facilitated the partial
187 equilibrium approach (PEA) to simulate redox reactions. At this point, PHREEQC
188 incorporates a virtual electron flow between the redox pairs, calculating,
189 automatically, *pe* every time step. The PEA approach has been successfully used for
190 simulating redox processes in MAR and comparable biogeochemical subsurface
191 systems[9, 15, 16, 20, 41, 44-46].

192 **2.3 Model set-up and calibration process**

193 To model the redox potential evolution in Castellbisbal, the site was simplified
194 behaving as one-dimensional with the top element varying for the different periods,
195 which incorporated the seasonal effects of clogging (decreasing in hydraulic
196 conductivity and increasing of SOM). The decreasing in hydraulic conductivity was
197 associated to a combination of clogging processes, although they were not explicitly
198 modelled individually: compaction, bioclogging or gas entrapment. Thus, the
199 developed flow, heat and reactive transport model consisted of a vertical profile from
200 the bottom of the infiltration pond to the groundwater (total length of 6 m),
201 discretized into 100 equispaced nodes. The total modeled time was one year, covering
202 the full period of continuous monitoring. Spatial and temporal discretizations were
203 selected according to Péclet and Courant criteria to avoid numerical oscillations.
204 The model geometry involved two zones, the top one of 24 cm and the bottom one of
205 576 cm. The top layer was intended to reproduce the combination of clogging effects
206 and scrapping operations described in Table 2, thus, with a variation of hydraulic
207 conductivity and Sedimentary Organic Matter (SOM). Consequently, the model was
208 divided into five sub-models (named P-I to P-V, see Table 2) where hydraulic
209 conductivity and SOM in the top layer changed in each one. Both parameters were
210 manually calibrated (Table 2), although in the case of SOM, we followed the tendency

observed in SOM concentration corresponding to the first 2 cm (see section S7). The hydraulic conductivity of the deeper layer remained constant in time.

Regarding the flow model boundaries, the water level of the infiltration pond was mostly specified as a Dirichlet condition for the top boundary. In August 2017, with the pond being empty from days 281 to 308, prescribed (null) flux was applied as upper boundary condition (BC). Evaporation was assumed negligible. The bottom BC was specified as constant head with the data measured in PJ (Fig-1 SI). For the initial conditions, we defined negative pressures in the unsaturated zone from the surface to the groundwater level, with a pressure of 0 (node 58, 3.42 cm), imposing a linear gradient of 0.359 cm/node. Porosity was fixed at 0.28, being the average of values reported in different local studies.

Afterwards, a heat transport model was built. The initial temperature profile was interpolated between the top node specified at constant temperature of 19°C (temperature of the infiltration water at time 0), and the bottom node, set at 20°C (temperature of water in the aquifer at t=0). Then, we applied the convection-dispersion equation (Eq. 5 in SI) to solve the heat transport. Temperature of the infiltration water and at the aquifer (PJ) were prescribed daily as upper and lower boundary conditions, respectively. The thermal parameters of the soil were set to default values provided by Chung and Horton (1987)[47] for a sandy material . The heat transport model was evaluated by comparing the temperature calculated at a depth of 55 cm with the data provided by the temperature sensor at this depth (probe 3, Figure S1).

Lastly, a reactive transport model was constructed. The geochemical signature of the initial and the inflow solutions are presented in section S4 of SI. The reactive transport model was calibrated manually, trying to get the best fit to the oxidation-reduction potential measured at the probes with respect to the Eh values provided

by the HP1 model, as well as to DOC, TEAPs, ammonium and pH recorded from the four hydrogeochemical campaigns. Calibration was focused on the first meter of the model domain, since this was the zone intensively monitored. To facilitate calibration, we set all the saturation constants as well as the inhibition parameters from the geochemical model fixed.

3 Results and discussion

3.1 A model capable of reproducing the Eh field measurements

The first step in the modeling effort was the coupled flow and heat transport model. Figure 2 shows that the model captured the main trends of the evolution of the infiltration with time, by manually calibrating the saturated hydraulic conductivity (K_s) in the top layer, ranging from 5 to 600 cm/d (Table 2). The lowest value was set at spring and summer (P-III), in agreement with the lowest infiltration rate due to clogging (flooding of the site during a rain event and non-scrapping for 6 months) and the algae bloom observed in the infiltration pond. A value of 600 cm/d of K_s was assigned to the top layer after scrapping (P-IV), equal to that for the bottom layer (not affected by clogging in our model). Nevertheless, this value decreased to 30 cm/d in less than one month (P-V), indicating that summer scrapping did not guarantee significant infiltration capacity for long.

Regarding the heat transport model, the model fitting for temperature is quite good at the depth of 55 cm (Figure 2b). Figure 3a shows the hydraulic conductivity (K_T) as a function of space and time, affected by the density and viscosity dependence on T (Eq.7 of SI) and by soil water content (Figure S2). The actual range of K_T values is quite large [1.42 x 10^{-2} -766] cm/d, with the lowest values taking place in winter,

affected by the low water content values, and the highest ones corresponding to fully saturated conditions in spring/summer, mainly affected by changes in viscosity and density.

The next step was building the full reactive transport model. Calibration was performed on a number of transport and reaction model parameters (Table S3, SI), as well as the initial amount of SOM in the surface layer corresponding to each model period (Table 2). Estimated SOM values correlated inversely with K, indicating that the former are also affected by seasonality, or in other words, that biomass growth played an important role in the source of SOM, being the electron donor in the system. Notice that the SOM calibrated values were much lower than the experimental ones (Figure S3), which is partially explained since the former were representative of the model top layer (24 cm) while the latter only referred to the top 2 cm. Nevertheless, they followed the same trend.

The geochemical model, fitted by considering both hydrochemistry and *Eh* data, captured the main evolution of redox related compounds and pH (Figure 4). In December, the system operated under aerobic conditions, with ammonium oxidizing to nitrate. The other TEAPs (nitrate, manganese, iron and sulfate) remained stable, indicating the poor activity of the system, probably because of low temperatures; indeed, the results are quite similar without organic matter degradation (dashed lines, Figure 4). In the subsequent three campaigns, all the TEAPs were activated and the system achieved reducing conditions: nitrate and sulfate were completely depleted, and Mn(II) and Fe(II) were produced. These observations were coherent with the dominating rates for the different periods (Figures 5 and Figure S4), whereas Mn-reduction dominated in winter and early spring, iron and sulfate-reductions were the driving processes during spring and summer. Iron and sulfate reduction coexistence was associated to the sulfate reduction due to the re-oxidation

of Fe(II)[40]. The activation of more reducing processes was clearly related with the SOM concentration increasing during the warm periods of the year, in line with the observations in infiltration ponds elsewhere[48, 49].

The Mn^{2+} and Fe^{2+} profiles were achieved by incorporating secondary processes into the model: precipitation of rhodochrosite and mackinawite, respectively, and cation exchange. These assumptions were based on previous work where the authors observed these minerals forming in batch redox experiments with similar sediments and groundwater[50]. Mackinawite precipitation was also identified in field campaigns (as a black sediment) and its formation has been described in similar works[50-53]. Although the model fitted the general tendency, in the April campaign, iron and pH fittings were not well adjusted, which we explain by heterogeneity in the system delaying the iron reducing front. On the other hand, despite several modelled scenarios showed mackinawite precipitation was the most significant process governing Fe(II), we did not neglect the impact of exchange processes with SOM (as the clay content in the soil was negligible) on iron dynamics.

Figure 5 shows the temporal evolution of the redox potential (mean plus/minus one standard deviation of the 120 daily measurements), together with the model results at different depths. The model fitted quite well the general tendency of the redox potential, showing the highest aerobic potentials (positive Eh values, also extending along the vertical) during the colder periods. This seasonality was associated to the amount of SOM as well as the increasing of geochemical reaction rates in the warmer periods. During the first weeks of Period-I, we observed some model discrepancies which were attributed to the stabilization of Eh sensors. Also note that Eh measurements were not compensated with pH since we did not have the same spatial/temporal resolution in the latter; moreover, pH variation ranged only about 1 unit. In general terms, the fittings were better for the deeper sensors (55, 62 and

313 70 cm), probably because deep fluxes are more homogeneous than those near the
314 surface. The model fitting indicates that the computation of pe performed by the PEA
315 in PHREEQC properly represents the Eh values measured by several sensors.

316 **3.2 Evaluating the influence of different processes upon the redox**
317 **potential**

318 In this section, we tested the significance of some processes in the resulting
319 geochemical model, emphasizing their impact upon the Eh data (Figure 6). For that,
320 we ran different scenarios, always compared to the model presented in the previous
321 section (termed E0). In the first alternative scenario (E1), we tested the effect of
322 temperature. It was divided in three sub-scenarios: E1.1 where we neglected the
323 impact of heat transport in flow and geochemical processes; here, temperature was
324 fixed at the average value of the whole domain (18ºC) for all times and depths; E1.2
325 where heat transport was considered but neglected in the reaction rates (constant F_T
326 assuming 18ºC) and E1.3. where heat transport was also neglected but F_T was
327 recalculated from the seasonal constant temperature introduced in each period. In
328 scenario E2, we neglected the role of SOM generation due to the photosynthetic
329 organisms; numerically, this implied setting the initial amount of SOM to 0 in all
330 five periods considered (recall Table 2). Finally, in scenario E3, we neglected all the
331 secondary processes associated to reduced iron and manganese geochemistry.

332 From these scenarios, the amount of organic matter (E2) is the most significant
333 variable for simulating the redox potential dynamics, since it is the main electron
334 donor driving the redox reactions. The fixation of CO_2 and the subsequent formation
335 of DOC is the main source of electrons, well above the DOC supplied by the recharge
336 water. Also, considering the effect of temperature in reaction rates (F_T) is relevant
337 (E1.3), even if a full heat transport model is not implemented. Indeed, the impact of
338 heat transport in water velocity did not modify significantly the modelled Eh (E1.1-

E1.2). Finally, note that E3 is quite similar to the reference scenario; we attribute it to secondary geochemical processes (precipitation and cation exchange) only affecting the fate of Mn^{+2}/Fe^{+2} but not the Eh, since these two components are already in reduced conditions.

3.3 Implications for reduction-oxidation potential monitoring in environmental systems

In this work we have shown that the reduction-oxidation potential measured under natural conditions with continuous and *in-situ* sensor probes can be reproduced by a geochemical model. This fact exhibits and confirms that the traditional Eh sampling methodology is not adequate to be incorporated into a mathematical model, since it is not valid and not representative of individual points; consequently, these measurements have hardly any possibility to be reproduced. In our case, in all sampling points, except the surface water, we observed a bias in Eh measurements (see section S9, Figure S5). In winter, traditional sampling led more reducing values compared with *in-situ* measurements, whereas in spring/summer periods more aerobic values were measured. Thus, the use of Eh non-invasive point sensors at different depths is quite recommendable, especially if a numerical reproduction of the site is required. We still recommend to combine this information with traditional hydrogeochemical sampling campaigns performed at different seasons, monitoring, at least, the TEAPs and the organic matter dynamics.

Our results also demonstrated that acknowledging the effects of temperature in reaction rates is crucial to reproduce Eh trends in space and time; thus, infiltration pond models should always account for the temperature factor (F_T) in geochemical rates. Consequently, it is high recommendable to install temperature sensors at different depths of the experimental sites in order to catch the seasonal evolution of

364 temperature. These recommendations are extended to similar models developed e.g.
365 in constructed wetlands or the hyporheic zone.

366 We found that the seasonal activity of photosynthetic organisms is a relevant factor
367 affecting both physical infiltration processes (via bioclogging) and the geochemical
368 redox processes (being a source of organic carbon and thus becoming a prime process
369 in the vertical distribution of redox potential).

370 Understanding the redox processes in an infiltration system is quite important to
371 assess the real purification capacity of a recharge facility, in particular regarding
372 emerging organic compounds. In this way, this work is a step-forward in the redox
373 characterization and process quantification which will allow to improve the
374 understanding of the fate of these compounds.

375

4 Supporting Information Available

Detailed site description; field site monitoring; model construction; tables of initial/boundary concentrations and fitted parameters of the reactive transport; and figures about the evolution of water content, evolution of Sedimentary Organic Matter, TEAPs rate's plume and comparison of different experimental Eh are available in the form of Supporting Information.

5 Acknowledgements

This work was financially supported by MONOPOLIOS (RTI2018-101990-B-100, MINECO/FEDER), the EU project MARADENTRO (PCI2019-103425-WW2017), the Catalan Research Project RESTORA (ACA210/18/00040) and AGAUR (AQU - 2017 SGR 1485). The authors wish to acknowledge Comunitat d'Usuaris d'Aigües de la Cubeta de Sant Andreu de la Barca (CUACSA) and the Agència Catalana de l'Aigua for their cooperation.

6 References

1. Appelo, C. A. J.; Postma, D., *Geochemistry, groundwater and pollution*. Balkema: 2005.
2. Lindberg, R. D.; Runnells, D. D., Ground Water Redox Reactions: An Analysis of Equilibrium State Applied to Eh Measurements and Geochemical Modeling. *Science* **1984,** *225*, (4665), 925.
3. Christensen, T. H.; Bjerg, P. L.; Banwart, S. A.; Jakobsen, R.; Heron, G.; Albrechtsen, H.-J., Characterization of redox conditions in groundwater contaminant plumes. *Journal of Contaminant Hydrology* **2000,** *45*, (3), 165-241.
4. Vorenhout, M.; van der Geest, H. G.; van Marum, D.; Wattel, K.; Eijsackers, H. J., Automated and continuous redox potential measurements in soil. *J Environ Qual* **2004,** *33*, (4), 1562-7.
5. Lee, P. O.; Shoemaker, C.; Olson, J. B., Wetland Soil Properties and Resident Bacterial Communities Are Influenced by Changes in Elevation. *Wetlands* **2019,** *39*, (1), 99-112.
6. Wallace, C. D.; Sawyer, A. H.; Barnes, R. T., Spectral analysis of continuous redox data reveals geochemical dynamics near the stream–aquifer interface. *Hydrological Processes* **2019,** *33*, (3), 405-413.
7. Vonk, J. A.; Rombouts, T.; Schoorl, J. C.; Serne, P.; Westerveld, J. W.; Cornelissen, P.; van der Geest, H. G., Impact of water drawdown and rewetting on sediment nutrient-dynamics in a constructed delta-lake system (Oostvaardersplassen, The Netherlands): A mesocosm study. *Ecol. Eng.* **2017,** *108*, 396-405.
8. Barba, C.; Folch, A.; Gaju, N.; Sanchez-Vila, X.; Carrasquilla, M.; Grau-Martínez, A.; Martínez-Alonso, M., Microbial community changes induced by Managed Aquifer Recharge activities: linking hydrogeological and biological processes. *Hydrol. Earth Syst. Sci.* **2019,** *23*, (1), 139-154.
9. Greskowiak, J.; Prommer, H.; Massmann, G.; Nützmann, G., Modeling Seasonal Redox Dynamics and the Corresponding Fate of the Pharmaceutical Residue Phenazone During Artificial Recharge of Groundwater. *Environ. Sci. Technol.* **2006,** *40*, (21), 6615-6621.
10. Massmann, G.; Pekdeger, A.; Merz, C., Redox processes in the Oderbruch polder groundwater flow system in Germany. *Appl. Geochem.* **2004,** *19*, (6), 863-886.
11. Dillon, P.; Stuyfzand, P.; Grischek, T.; Lluria, M.; Pyne, R. D. G.; Jain, R. C.; Bear, J.; Schwarz, J.; Wang, W.; Fernandez, E.; Stefan, C.; Pettenati, M.; van der Gun, J.; Sprenger, C.; Massmann, G.; Scanlon, B. R.; Xanke, J.; Jokela, P.; Zheng, Y.; Rossetto, R.; Shamrukh, M.; Pavelic, P.; Murray, E.; Ross, A.; Bonilla Valverde, J. P.; Palma Nava, A.; Ansems, N.; Posavec, K.; Ha, K.; Martin, R.; Sapiano, M., Sixty years of global progress in managed aquifer recharge. *Hydrogeol. J.* **2018,** 27, 1-30.
12. Rodríguez-Escales, P.; Canelles, A.; Sanchez-Vila, X.; Folch, A.; Kurtzman, D.; Rossetto, R.; Fernández-Escalante, E.; Lobo-Ferreira, J. P.; Sapiano, M.; San-Sebastián, J.; Schüth, C., A risk assessment methodology to evaluate the risk failure of managed aquifer recharge in the Mediterranean Basin. *Hydrol. Earth Syst. Sci.* **2018,** *22*, (6), 3213-3227.
13. Li, D.; Sharp, J. O.; Saikaly, P. E.; Ali, S.; Alidina, M.; Alarawi, M. S.; Keller, S.; Hoppe-Jones, C.; Drewes, J. E., Dissolved Organic Carbon Influences Microbial Community Composition and Diversity in Managed Aquifer Recharge Systems. *Appl. Environ. Microb.* **2012,** *78*, (19), 6819.

14. Rolle, M.; Clement, T. P.; Sethi, R.; Di Molfetta, A., A kinetic approach for simulating redox-controlled fringe and core biodegradation processes in groundwater: model development and application to a landfill site in Piedmont, Italy. *Hydrol. Proces.* **2008,** *22*, (25), 4905-4921.
15. Rodríguez-Escales, P.; Folch, A.; van Breukelen, B. M.; Vidal-Gavilan, G.; Sanchez-Vila, X., Modeling long term Enhanced in situ Biodenitrification and induced heterogeneity in column experiments under different feeding strategies. *J. Hydrol.* **2016,** *538*, 127-137.
16. Rodríguez-Escales, P.; Folch, A.; Vidal-Gavilan, G.; van Breukelen, B. M., Modeling biogeochemical processes and isotope fractionation of enhanced in situ biodenitrification in a fractured aquifer. *Chem. Geol.* **2016,** *425*, 52-64.
17. Barba, C.; Folch, A.; Sanchez-Vila, X.; Martínez-Alonso, M.; Gaju, N., Are dominant microbial sub-surface communities affected by water quality and soil characteristics? *Journal of Environmental Management* **2019,** *237*, 332-343.
18. van Breukelen, B. M.; Griffioen, J.; Röling, W. F. M.; van Verseveld, H. W., Reactive transport modelling of biogeochemical processes and carbon isotope geochemistry inside a landfill leachate plume. *J. Contam. Hydrol.* **2004,** *70*, (3–4), 249-269.
19. Greskowiak, J.; Hamann, E.; Burke, V.; Massmann, G., The uncertainty of biodegradation rate constants of emerging organic compounds in soil and groundwater – A compilation of literature values for 82 substances. *Water Res.* **2017,** *126*, 122-133.
20. Rodríguez-Escales, P.; Fernàndez-Garcia, D.; Drechsel, J.; Folch, A.; Sanchez-Vila, X., Improving degradation of emerging organic compounds by applying chaotic advection in Managed Aquifer Recharge in randomly heterogeneous porous media. *Water Resour. Res.* **2017,** *53*, (5), 4376-4392.
21. Rodríguez-Escales, P.; Sanchez-Vila, X., Modeling the fate of UV filters in subsurface: Co-metabolic degradation and the role of biomass in sorption processes. *Water Res.* **2019**, 115192.
22. Rodríguez-Escales, P.; Sanchez-Vila, X., Fate of sulfamethoxazole in groundwater: Conceptualizing and modeling metabolite formation under different redox conditions. *Water Res.* **2016,** *105*, 540-550.
23. Freixa, A.; Rubol, S.; Carles-Brangarí, A.; Fernàndez-Garcia, D.; Butturini, A.; Sanchez-Vila, X.; Romaní, A. M., The effects of sediment depth and oxygen concentration on the use of organic matter: An experimental study using an infiltration sediment tank. *Sci. Tot. Environ.* **2016,** *540*, 20-31.
24. Rivett, M. O.; Buss, S. R.; Morgan, P.; Smith, J. W. N.; Bemment, C. D., Nitrate attenuation in groundwater: A review of biogeochemical controlling processes. *Water Res.* **2008,** *42*, (16), 4215-4232.
25. Panno, S. V.; Kelly, W. R.; Hackley, K. C.; Hwang, H.-H.; Martinsek, A. T., Sources and fate of nitrate in the Illinois River Basin, Illinois. *J. Hydrol.* **2008,** *359*, (1–2), 174-188.
26. Dou, M.; Ma, X.; Zhang, Y.; Zhang, Y.; Shi, Y., Modeling the interaction of light and nutrients as factors driving lake eutrophication. *Ecol. Mod.* **2019,** *400*, 41-52.
27. Dutta, T.; Carles-Brangarí, A.; Fernàndez-Garcia, D.; Rubol, S.; Tirado-Conde, J.; Sanchez-Vila, X., Vadose zone oxygen (O2) dynamics during drying and wetting cycles: An artificial recharge laboratory experiment. *J. Hydrol.* **2015,** *527*, 151-159.
28. Pedretti, D.; Barahona-Palomo, M.; Bolster, D.; Sanchez-Vila, X.; Fernàndez-Garcia, D., A quick and inexpensive method to quantify spatially variable

infiltration capacity for artificial recharge ponds using photographic images. *J. Hydrol.* **2012,** *430–431*, 118-126.
29. Massmann, G.; Greskowiak, J.; Dünnbier, U.; Zuehlke, S.; Knappe, A.; Pekdeger, A., The impact of variable temperatures on the redox conditions and the behaviour of pharmaceutical residues during artificial recharge. *J. Hydrol.* **2006,** *328*, (1), 141-156.
30. Henzler, A. F.; Greskowiak, J.; Massmann, G., Seasonality of temperatures and redox zonations during bank filtration – A modeling approach. *J. Hydrol.* **2016,** *535*, 282-292.
31. Greskowiak, J.; Prommer, H.; Vanderzalm, J.; Pavelic, P.; Dillon, P., Modeling of carbon cycling and biogeochemical changes during injection and recovery of reclaimed water at Bolivar, South Australia. *Water Resour. Res.* **2005,** *41*, (10), W10418.
32. Prommer, H.; Stuyfzand, P. J., Identification of Temperature-Dependent Water Quality Changes during a Deep Well Injection Experiment in a Pyritic Aquifer. *Environ. Sci. Technol.* **2005,** *39*, (7), 2200-2209.
33. Seibert, S.; Atteia, O.; Ursula Salmon, S.; Siade, A.; Douglas, G.; Prommer, H., Identification and quantification of redox and pH buffering processes in a heterogeneous, low carbonate aquifer during managed aquifer recharge. *Water Resour. Res.* **2016,** *52*, (5), 4003-4025.
34. Schafer, D.; Sun, J.; Jamieson, J.; Siade, A. J.; Atteia, O.; Prommer, H., Model-Based Analysis of Reactive Transport Processes Governing Fluoride and Phosphate Release and Attenuation during Managed Aquifer Recharge. *Environ. Sci. Technol.* **2020,** *54*, (5), 2800-2811.
35. Greskowiak, J.; Prommer, H.; Massmann, G.; Johnston, C. D.; Nützmann, G.; Pekdeger, A., The impact of variably saturated conditions on hydrogeochemical changes during artificial recharge of groundwater. *Appl. Geochem.* **2005,** *20*, (7), 1409-1426.
36. Diederik, J.; Jiří, Š.; Dirk, M.; Martinus Th. van, G., The HPx software for multicomponent reactive transport during variably-saturated flow: Recent developments and applications. *J. Hydrol. Hydromech.* **2018,** *66*, (2), 211-226.
37. Jacques, D.; Šimůnek, J.; Mallants, D.; van Genuchten, M. T., Modeling Coupled Hydrologic and Chemical Processes: Long-Term Uranium Transport following Phosphorus Fertilization. *Vadose Zone J.* **2008,** *7*, (2), 698-711.
38. Šimůnek, J.; van Genuchten, M. T.; Šejna, M., HYDRUS: Model use, calibration and validation, Special issue on Standard/Engineering Procedures for Model Calibration and Validation,. *Transactions of the ASABE* **2012,** *55(4)*, 13.
39. Parkhurst, D. L.; Appelo, C. A. J. *User's guide to PHREEQC (version 2) - a computer program for speciation, reaction-path, 1D-transport, and inverse geochemical calculations.*; U.S. GEOLOGICAL SURVEY: 1999.
40. Postma, D.; Jakobsen, R., Redox zonation: Equilibrium constraints on the Fe(III)/SO4-reduction interface. *Geochim. Cosmochim. Ac.* **1996,** *60*, (17), 3169-3175.
41. Brun, A.; Engesgaard, P., Modelling of transport and biogeochemical processes in pollution plumes: literature review and model development. *J. Hydrol.* **2002,** *256*, (3–4), 211-227.
42. O'Connell, A. M., Microbial decomposition (respiration) of litter in eucalypt forests of South-Western Australia: An empirical model based on laboratory incubations. *Soil Biol. Biochem.* **1990,** *22*, (2), 153-160.
43. Palandri, J. L.; Kharaka, Y. K. *A compilation of rate parameters of water-mineral interaction kinetics interaction for application to geochemical modeling*; U.S. GEOLOGICAL SURVEY: 2004.

44. Prommer, H.; Tuxen, N.; Bjerg, P. L., Fringe-controlled natural attenuation of phenoxy acids in a landfill plume: integration of field-scale processes by reactive transport modeling. *Environ. Sci. Technol.* **2006,** *40*, (15), 4732-8.
45. Prommer, H.; Grassi, M. E.; Davis, A. C.; Patterson, B. M., Modeling of Microbial Dynamics and Geochemical Changes in a Metal Bioprecipitation Experiment. *Environ. Sci. Technol.* **2007,** *41*, (24), 8433-8438.
46. Jakobsen, R.; Postma, D., Redox zoning, rates of sulfate reduction and interactions with Fe-reduction and methanogenesis in a shallow sandy aquifer, Rømø, Denmark. *Geochim. Cosmochim. Ac.* **1999,** *63*, (1), 137-151.
47. Chung, S.-O.; Horton, R., Soil heat and water flow with a partial surface mulch. *Water Resources Research* **1987,** *23*, (12), 2175-2186.
48. Grau-Martínez, A.; Folch, A.; Torrentó, C.; Valhondo, C.; Barba, C.; Domènech, C.; Soler, A.; Otero, N., Monitoring induced denitrification during managed aquifer recharge in an infiltration pond. *J. Hydrol.* **2018,** *561*, 123-135.
49. Barba, C. Physical, geochemical and microbial parameters driving the improvement of water quality in Managed Aquifer Recharge. Universitat Politècnica de Catalunya, Barcelona, 2018.
50. Barbieri, M.; Carrera, J.; Sanchez-Vila, X.; Ayora, C.; Cama, J.; Köck-Schulmeyer, M.; López de Alda, M.; Barceló, D.; Tobella Brunet, J.; Hernández García, M., Microcosm experiments to control anaerobic redox conditions when studying the fate of organic micropollutants in aquifer material. *J. Contam. Hydrol.* **2011,** *126*, (3–4), 330-345.
51. Rickard, D.; Luther, G. W., Chemistry of Iron Sulfides. *Chem. Rev.* **2007,** *107*, (2), 514-562.
52. Williams, K. H.; Kemna, A.; Wilkins, M. J.; Druhan, J.; Arntzen, E.; N'Guessan, A. L.; Long, P. E.; Hubbard, S. S.; Banfield, J. F., Geophysical Monitoring of Coupled Microbial and Geochemical Processes During Stimulated Subsurface Bioremediation. *Environ. Sci. Technol.* **2009,** *43*, (17), 6717-6723.
53. Van Cappellen, P.; Wang, Y., Cycling of iron and manganese in surface sediments; a general theory for the coupled transport and reaction of carbon, oxygen, nitrogen, sulfur, iron, and manganese. *Am. J. Sci.* **1996,** *296*, (3), 197-243.

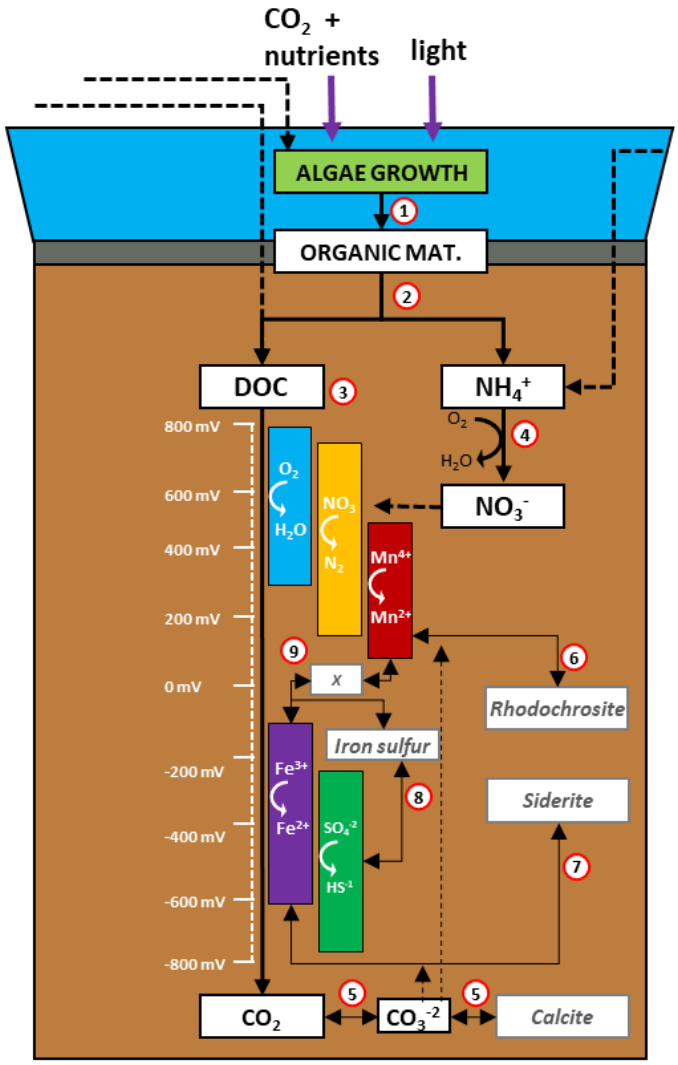

576

577 **Figure 1.** Biogeochemical processes considered in the reactive transport model of the Castellbisbal
578 infiltration pond: 1) organic matter (OM) generation; 2) OM decay; 3) organic carbon oxidation with
579 different TEAPs; 4) nitrification; 5) carbonate equilibrium and calcite precipitation; 6) rhodochrosite
580 formation and precipitation; 7) siderite formation and precipitation; 8) iron sulfur and precipitation (in
581 form of mackinawite); and 9) Cation Exchange on soil exchange complex (X) with iron and manganese.
582 The image shows an algae bloom generated in the infiltration pond during low flow conditions
583 highlighting the intensive biological activity (May 2017).

584

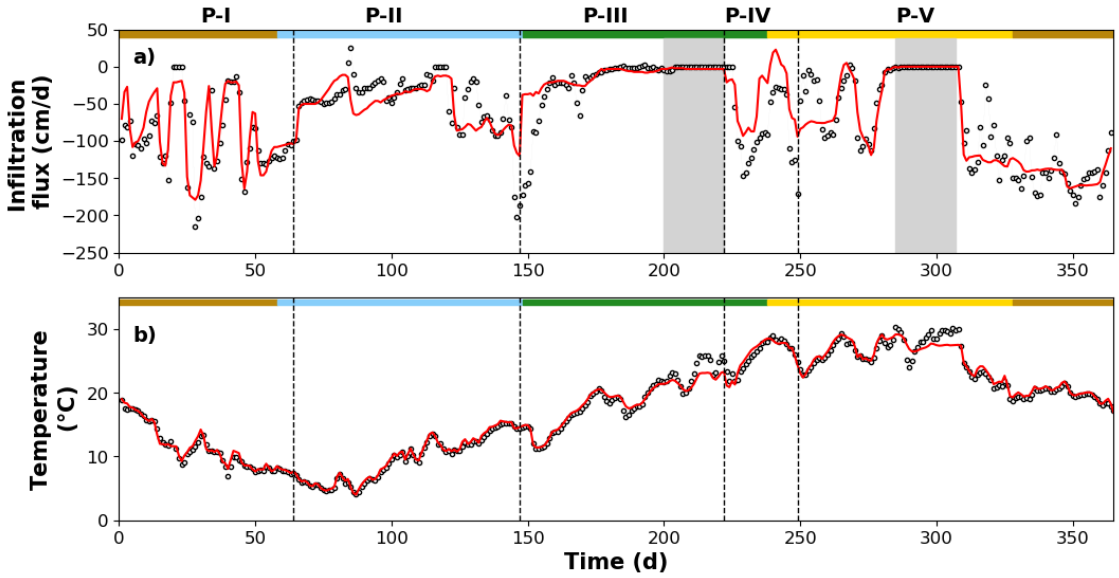

Figure 2. a) Evolution of infiltrating flow rate; b) Temperature evolution at 55 cm depth during the five modeled periods. The red lines are the result of the coupled flow and heat transport model, and the black points the experimental data. The season evolution is described in the top bar using a color code: brown for fall, blue for winter, green for spring, and yellow for summer. The grey zones represent periods when recharge was discontinued, the first one for scrapping actions; in the second one the pond was dry.

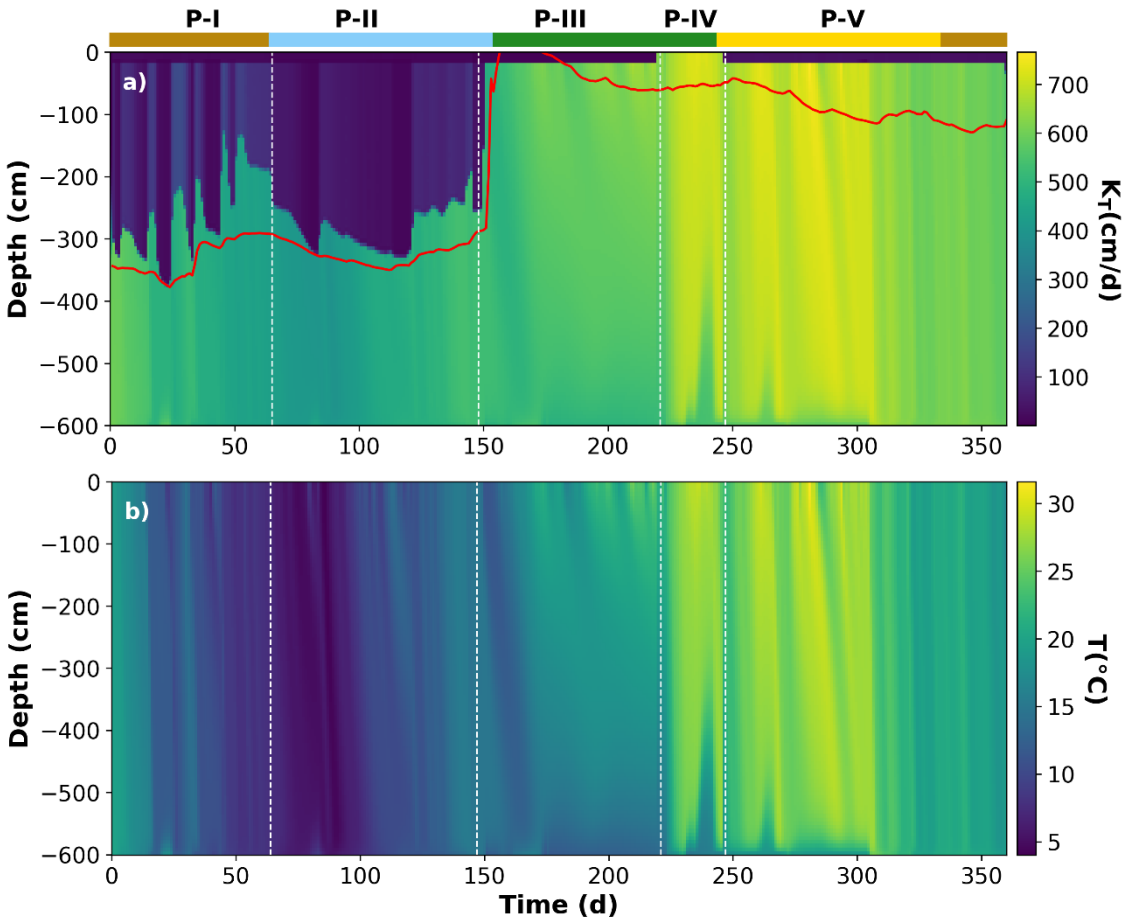

Figure 3. Variation of effective hydraulic conductivity (a), and temperature (b) with depth as a function of time. The season evolution is described in the top bar, similar to Figure 2. The red line in panel a) reflects the groundwater level evolution measured in PJ.

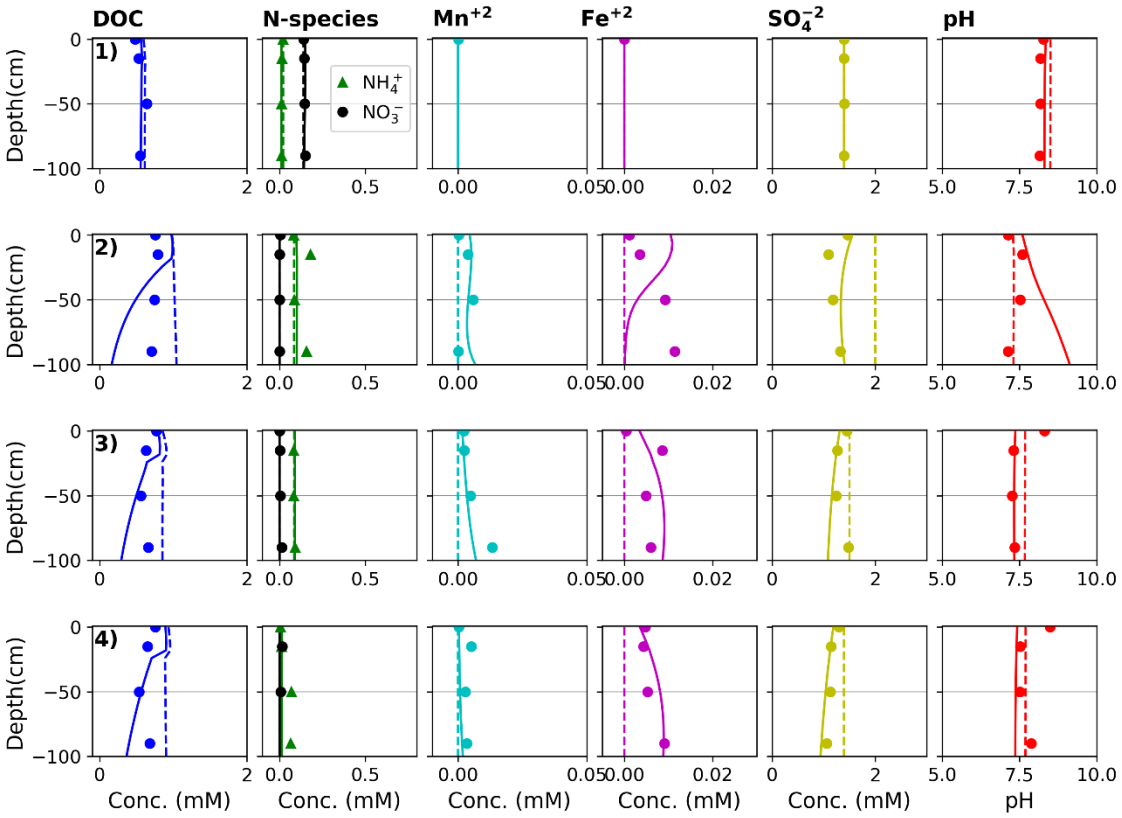

598

599 **Figure 4.** Evolution of DOC, ammonium and TEAPs in the four sampling campaigns. Points indicate
600 experimental data and solid lines are values supplied by the model. Dashed lines are the result model
601 without considering DOC degradation. Each row corresponds to one sampling campaign; from top to
602 bottom: December 2016, April 2017, June 2017, and July 2017.

603

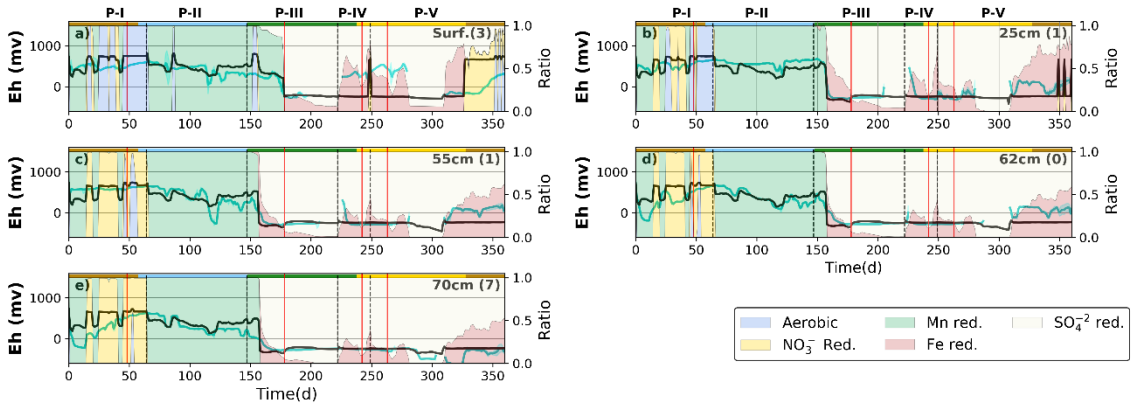

Figure 5. Evolution in time of redox potential at different depths (from the surface to 70 cm depth). The blue line represents the daily arithmetic average value of redox potential (from measurements taken every 12 min), presented as an area bounded by the plus/minus one standard deviation (hardly visible in most points). The redox potential information during dry periods is not shown since the redox sensor probe had high erratic oscillations due to low connectivity. The black line represents the model results. The red vertical lines represent the sampling dates for hydrochemistry. The background color of the plot reflects the relative importance of the different reaction rates in the total degradation of DOC. This importance (ratio) was calculated by dividing each rate by the sum of the total rates involved in TEAPs reduction.

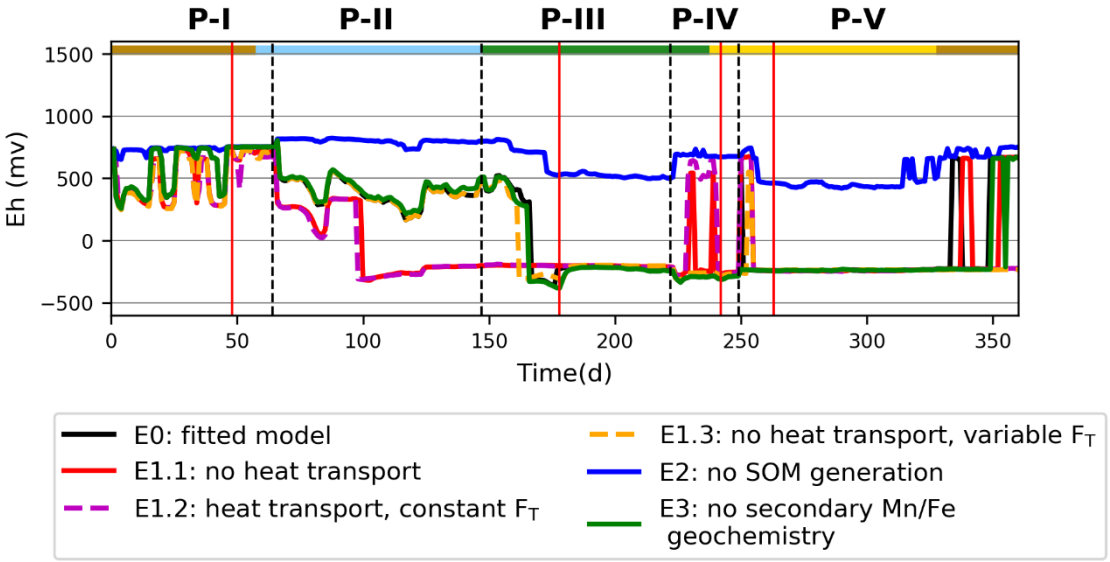

Figure 6. Sensitivity of the model response for Eh evolution as a function of time at the surface of the infiltration pond when including some alternative models neglecting one or more processes.

621 **Table 1.** Summary of processes, reactions, and rates in the reactive transport model. An extended
622 version of this table, with all the stoichiometric relationships and parameter description can be found
623 in the SI.

Process (reaction)	Kinetic rate	Equilibrium constant ($log\ K$)
Particulate organic matter generation from algae decomposition	$k_{gen} C_{SOM}\ F_T$	[-]
Degradation of particulate organic matter and dissolved organic carbon and ammonia generation	$k_{deg} C_{SOM} \left(\frac{C_{sat} + C_{DOC}}{C_{sat}}\right)\ F_T$	[-]
Nitrification $2NH_4^+ + 4O_2 \rightarrow 2NO_3^- + 4H^+ + 2H_2O$	$k_{nit} \frac{C_{NH_4^+}}{C_{NH_4^+} + K_{sat,NH_4^+}} \frac{C_{NO_3^-}}{C_{NO_3^-} + K_{sat,NO_3^-}} F_T$	[-]
Oxidation of organic carbon from different TEAPs		
$CH_2O + O_2 \rightarrow HCO_3^- + H^+$ $CH_2O + 0.8NO_3^- \rightarrow HCO_3^- + 0.4\ N_2 + 0.2H^+ + 0.4\ H_2O$ $2CH_2O + 4MnO_2 + 6H^+ \rightarrow 2HCO_3^- + 4Mn^{+2} + 4H_2O$ $CH_2O + 4FeO(OH) + 7H^+ \rightarrow HCO_3^- + 4\ Fe^{+2} + 6H_2O$ $2CH_2O + SO_4^{-2} \rightarrow HCO_3^- + HS^- + H^+$	$C_{DOC} \sum_{i=1}^{n} \left(k_i \frac{C_{EA}}{C_{EA} + K_{sat,EA}} \prod_{j=1}^{m} \frac{C_{j,EA} + K_{inh,j,AE}}{K_{inh,j,EA}} \right) \mathrm{F_T}$	[-]
Secondary mineral reactions		
Calcite precipitation $CaCO_3 \leftrightarrow Ca^{+2} + CO_3^{-2}$	$k_{Cc} \left(\frac{m_{Cc}}{m_{0,Cc}}\right)^{0.6} p\ (1 - \Omega_{\mathrm{Cc}})^{0.6}$	[-]
Rhodochrosite precipitation $MnCO_3 \leftrightarrow Mn^{+2} + CO_3^{-2}$	$k_{Rhod}(1 - \Omega_{\mathrm{Rhod}}) F_{T_{Ar}}$	[-]
Iron sulfur precipitation $FeS \leftrightarrow Fe^{+2} + S^{-2}$	$k_{Mack}(1 - \Omega_{\mathrm{Mack}}) F_{T_{Ar}}$	[-]
Siderite $FeCO_3 \leftrightarrow Fe^{+2} + CO_3^{-2}$	[-]	-10.89
Cation Exchange Reactions $Cat^{+i} + iX^-$ $\leftrightarrow CatX_i; Cat\{Na^+, K^+, NH_4^+, Ca^{+2}, Mg^{+2}, Mn^{+2}, Fe^{+2}\}$	[-]	various

624

625

626 **Table 2.** Periods considered in the model and fitted values of hydraulic conductivity and SOM
627 concentration of the top layer.
628

	Starting date	Duration (final day)	Characteristics	Surface layer	
				K (cm/d)	Sedimentary Organic Matter (M)*
P-I	24/10/16	64	Initial conditions	25	0.25
P-II	27/12/16	83 (147)	Intermediate infiltration rate Period ended with a heavy rainfall event	15	0.41
P-III	20/03/17	75 (222)	Low infiltration rate Physical and biological clogging	5	1.15
P-IV	03/06/17	27 (249)	Period after scrapping High infiltration rate	600	0.08
P-V	30/06/17	116 (365)	Fluctuation of infiltration rate Flow discontinued in the middle of the period (01-31/08/2017)	30	0.25

629 (*) SOM concentrations were transformed to mol/L considering a porosity of 0.28 and a soil density of
630 1.7 kg/L.